Photon Structure and the Production of Jets, Hadrons, and Prompt Photons

Michael Klasen

HEP Theory Group, Argonne National Laboratory, Argonne, IL 60439, USA

Abstract. We give a pedagogical introduction to hard photoproduction processes at HERA, including the production of jets, hadrons, and prompt photons. Recent theoretical developments in the three areas are reviewed.

1 Introduction

Electron-proton scattering at HERA proceeds dominantly through the exchange of a single photon with small virtuality $Q \simeq 0$. In this photoproduction limit and in the presence of a hard factorization scale $M_{\gamma,p}$, the electron-proton scattering cross section can be decomposed into

$$\mathrm{d}\sigma_{ep} = \sum_{a,b} \int_0^1 \mathrm{d}y F_{\gamma/e}(y, Q^2_{\mathrm{max}}) \int_0^1 \mathrm{d}x_\gamma F_{a/\gamma}(x_\gamma, M^2_\gamma) \int_0^1 \mathrm{d}x_p F_{b/p}(x_p, M^2_p) \mathrm{d}\sigma^{(n)}_{ab}. \tag{1}$$

The Weizsäcker-Williams spectrum of photons in the electron

$$F_{\gamma/e}(y, Q^2_{\mathrm{max}}) = \frac{\alpha}{2\pi} \left[\frac{1+(1-y)^2}{y} \ln\left(\frac{Q^2_{\mathrm{max}}}{Q^2_{\mathrm{min}}}\right) + 2m_e^2 y \left(\frac{1}{Q^2_{\mathrm{max}}} - \frac{1}{Q^2_{\mathrm{min}}}\right) \right] \tag{2}$$

is proportional to the electromagnetic coupling constant α. Since the photon virtuality is small, the spectrum can be calculated explicitly by exploiting current conservation and integrating over the unobserved azimuthal angle of the outgoing electron and over the virtuality of the photon. $Q^2_{\mathrm{min}} = m_e^2 y^2/(1-y)$ depends on the electron mass m_e and the longitudinal momentum fraction y of the photon in the electron. $Q^2_{\mathrm{max}} = E_e^2(1-y)\theta^2$ is determined experimentally from the incoming electron beam energy E_e, the momentum fraction y, and the scattering angle of the outgoing electron θ.

From deep inelastic scattering (DIS) experiments of virtual photons off protons it is well known that the proton has point-like constituents, quarks q and gluons g, also called partons. As the photon virtuality decreases, the photon itself begins to fluctuate into quark-antiquark ($q\overline{q}$) pairs, which in turn evolve into a vector meson-like structure. At HERA, an almost real photon radiated from the electron can thus interact either directly with the partons in the proton (direct component) or act as a hadronic source of partons which collide with the partons in the proton (resolved component). In the latter case, one does not test the proton structure alone but also the photon structure. Unfortunately, both

the photon and the proton structure cannot be calculated theoretically, but have to be determined experimentally.

Before HERA started taking data, information on the parton densities in the photon $F_{a/\gamma}$ came almost exclusively from deep inelastic $\gamma^*\gamma$ scattering at e^+e^- colliders. Whereas the singlet quark densities can be well constrained in this process, it is difficult to obtain information on the gluon density, which is suppressed relative to the quark densities by the strong coupling constant α_s. The gluon density can, however, be constrained from hard photoproduction processes at HERA if the direct contribution is suppressed by measuring the production of jets, hadrons, or prompt photons at low transverse energies E_T. This constitutes an important goal in studies of hard photoproduction.

Among the parton densities in the proton $F_{b/p}$, the quark densities and the gluon density at low x_p are rather well known today from DIS experiments. Of particular interest in photoproduction is the gluon distribution in the proton at large x_p. There, the experimental information from high-E_T jet and prompt photon production in hadron collisions is inconclusive and has considerable potential for improvement from lepton pair production in hadron collisions and from high-E_T photoproduction processes. At large E_T, the direct photoproduction process dominates and uncertainties from the photon structure are suppressed.

In the presence of a hard renormalization scale $\mu \simeq E_T$, $\alpha_s(\mu^2)$ becomes small and the partonic cross section

$$\mathrm{d}\sigma_{ab}^{(n)} = \alpha_s^0(\mu^2)\mathrm{d}\sigma_{ab}^{(0)} + \alpha_s^1(\mu^2)\mathrm{d}\sigma_{ab}^{(1)} + \ldots \tag{3}$$

for the scattering of two partons a and b, which can be quarks, gluons, and – in the photon case – also photons, into jets, hadrons, and prompt photons can be calculated in perturbative quantum chromodynamics (QCD). Testing these predictions constitutes a third goal for photoproduction experiments.

Typical leading order (LO) QCD diagrams for the direct and resolved photoproduction of jets are shown in the first line of Fig. 1. Next-to-leading order (NLO) QCD corrections to these graphs arise from virtual loop and real emission diagrams and have been calculated in [1]. The direct and resolved partonic processes are of $\mathcal{O}(\alpha\alpha_s)$ and $\mathcal{O}(\alpha_s^2)$, respectively. Since the parton densities in the photon are of $\mathcal{O}(\alpha/\alpha_s)$ in the asymptotic limit of large M_γ^2, both processes contribute at $\mathcal{O}(\alpha\alpha_s)$. In addition to the goals of photoproduction studies mentioned above, the observation of jets also permits to test and improve jet algorithms of both the cone and cluster types and to study jet profiles and the internal jet structure.

The LO partonic QCD diagrams for photoproduction of hadrons (second line in Fig. 1) are identical to those for the photoproduction of jets, and the NLO corrections for inclusive hadron production have been calculated in [2]. However, in this case the hadronic cross section

$$\mathrm{d}\sigma_{ab\to h}^{(n)} = \int_0^1 \frac{\mathrm{d}z}{z^2} D_{c/h}(z, M_h^2)\mathrm{d}\sigma_{ab\to c}^{(n)} \tag{4}$$

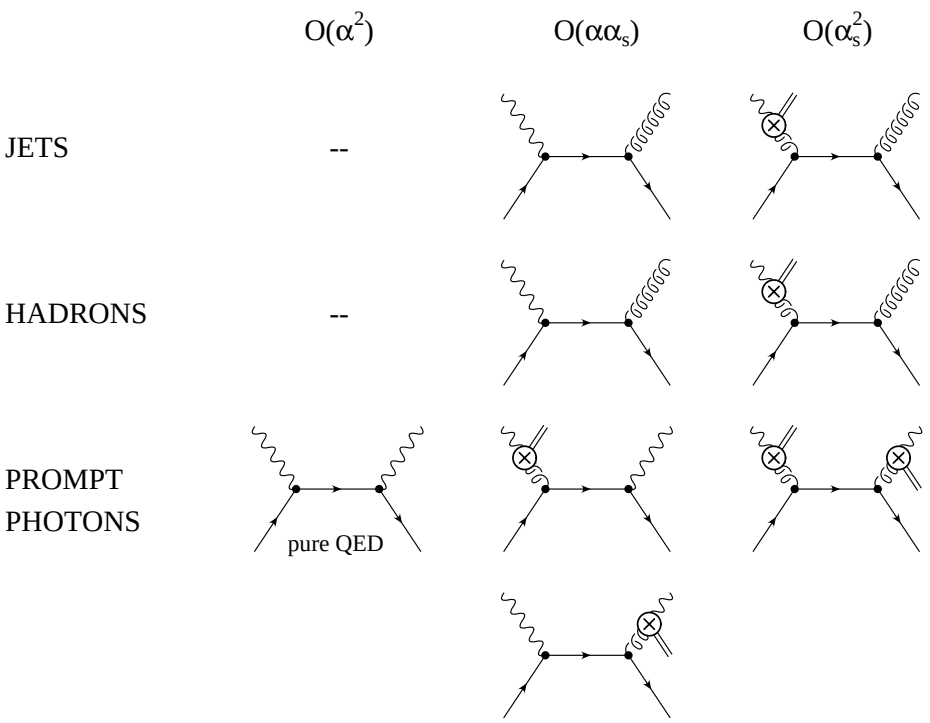

Fig. 1. Typical leading order QCD diagrams for the direct and resolved photoproduction of jets, hadrons, and prompt photons by order of the partonic scattering process. The $\mathcal{O}(\alpha^2)$ process is only present for the photoproduction of prompt photons

is obtained from the partonic cross section $\mathrm{d}\sigma_{ab\to c}$ by convoluting it with a fragmentation function $D_{c/h}$. Like parton distribution functions, fragmentation functions cannot be derived from first principles, and photoproduction of hadrons at HERA offers the additional possibility to test hadron fragmentation functions obtained, *e.g.*, in fits to data from e^+e^- colliders.

Like initial state photons, final state (prompt) photons couple to the hard partonic scattering process either directly or through their partonic constituents. The direct (lower left diagram in Fig. 1), single-resolved (center), and double-resolved (right) prompt photon processes contribute at different orders of the hard scattering process, but eventually the photon structure and fragmentation functions compensate for these differences so that all three subprocess types are effectively of $\mathcal{O}(\alpha^2)$. Comparable to hadron fragmentation functions, the partonic content of final state photons is described by a photon fragmentation function $D_{c/\gamma}$. Photoproduction of isolated photons and photons in association with jets has been calculated in NLO QCD in [3]. Since prompt photon production is a purely electromagnetic process in LO, its cross section is smaller than the

inclusive jet and hadron cross sections, and data from H1 and ZEUS have only recently become available.

2 Jets

At the first Ringberg workshop on "New Trends in HERA Physics" in 1997, photoproduction of jets had already been studied for five years. Several NLO single jet and the first NLO dijet calculations had been compared to data from H1 and ZEUS [4]. Studies of jet cross sections [5] and jet shapes [6] had demonstrated that the commonly used Snowmass jet cone algorithm [7] suffered from theoretical (double counting, parton distance) and experimental (seed finding, jet overlap) ambiguities, which could only be resolved by the introduction of a phenomenological parton distance parameter $R_{\rm sep}$ in addition to the cone size parameter R.

These ambiguities were found to be absent in the k_T-clustering algorithm in the inclusive mode [8], which has been used by the HERA experiments since then. It combines two hadronic clusters i and j if their distance

$$d_{ij} = \min(E_{T,i}^2, E_{T,j}^2)[(\eta_i - \eta_j)^2 + (\phi_i - \phi_j)^2]/R^2 \tag{5}$$

is smaller than E_T^2. The parameter $R = 1$ now corresponds to the parton distance parameter $R_{\rm sep}$ in NLO QCD. As in the cone algorithm, the transverse energy E_T, rapidity η, and azimuthal angle ϕ of the combined cluster are calculated from the transverse energy weighted sums of the two pre-clusters.

Three different NLO dijet calculations have recently been compared to ZEUS dijet data (see contribution by L. Sinclair to these proceedings) [9]. The definition of the ZEUS dijet cross section has also served as a basis to compare the theoretical predictions among themselves [10]. As can be seen in Fig. 2, the NLO transverse energy distributions agree with each other within the statistical accuracy of the Monte Carlo integration, which is about $\pm 1\%$ at low E_T for the full y range and $\pm 2\%$ for the high y range.

NLO dijet calculations involve the calculation of one-loop $2 \to 2$ and tree-level $2 \to 3$ scattering matrix elements. The latter are then integrated over soft and collinear regions of phase space in order to cancel the infrared divergences arising from the virtual corrections. If used in their original, unintegrated form, the $2 \to 3$ matrix elements can also be used for LO predictions of three jet cross sections. The three NLO dijet predictions mentioned above have also been applied to LO three jet cross sections and found to agree with each other [10]. ZEUS have measured the photoproduction of three jets with transverse energies larger than 6 GeV (two highest jets) and 5 GeV (third jet) and rapidities $|\eta| < 2.4$ [11]. Fig. 3 shows that the total theoretical prediction (full curve) describes the data well in shape and normalization [12]. The agreement in normalization is, however, to some degree coincidental since there is still an uncertainty of a factor of two from the variation of the scales $\mu = M_\gamma = M_p \in [0.5; 2.0] \times \max(E_{T,1}, E_{T,2}, E_{T,3})$ (shaded band). In these LO QCD predictions every parton corresponds to a jet, but a jet definition still has to be implemented for the

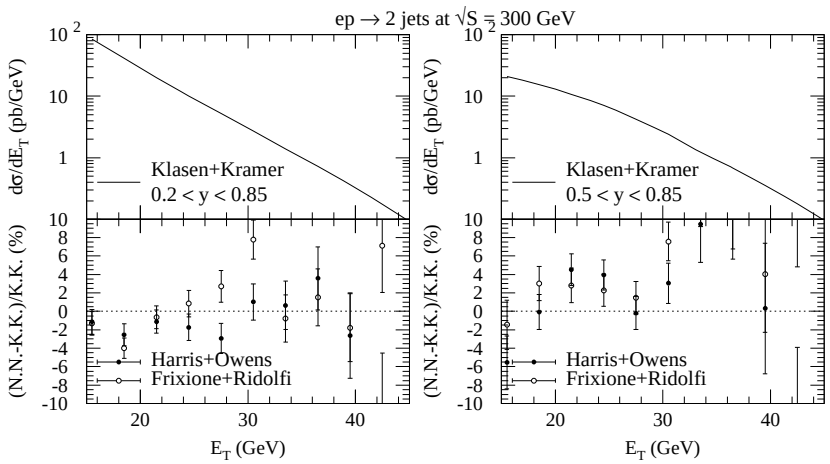

Fig. 2. Comparison of three theoretical predictions for the NLO dijet cross section as a function of the transverse energy E_T of the leading jet for the full (left) and high (right) y range. Both jets lie in a central rapidity range $0 < \eta_{1,2} < 1$

condition that two partons cannot come closer too each other than permitted by the jet algorithm.

H1 have recently analyzed the production of dijets with transverse momentum $p_T > 4$ and 6 GeV, dijet mass $M_{2-\mathrm{jet}} > 12$ GeV, rapidities $-0.5 < \eta_{1,2} < 2.5, |\eta_1 - \eta_2| < 1$, and photon energy fraction $0.5 < y < 0.7$ as a function of the variable

$$x_\gamma^{\mathrm{jets}} = \sum_{i=1}^{2} E_{T,i} e^{-\eta_i} / (y\sqrt{S}). \tag{6}$$

This variable can be determined from the two observed jets and is, in LO QCD, directly related to the momentum fraction of the parton in the photon. H1 have used this measurement of the dijet cross section to extract the gluon density in the photon with the result shown in Fig. 4. The 1996 data [13] are consistent with older H1 charged track [14] and jet [15] measurements. They agree very well with the GRV parametrization [16], but rule out both the LAC1 [17] and LAG parametrizations [18] of the gluon density. The systematic (outer) error bars include theoretical uncertainties coming from the variation of different Monte Carlo models, parton densities in the proton, and quark densities in the photon.

3 Hadrons

The transformation of quarks and gluons into hadronic final states can be described globally by jet definitions. More detailed experimental information about

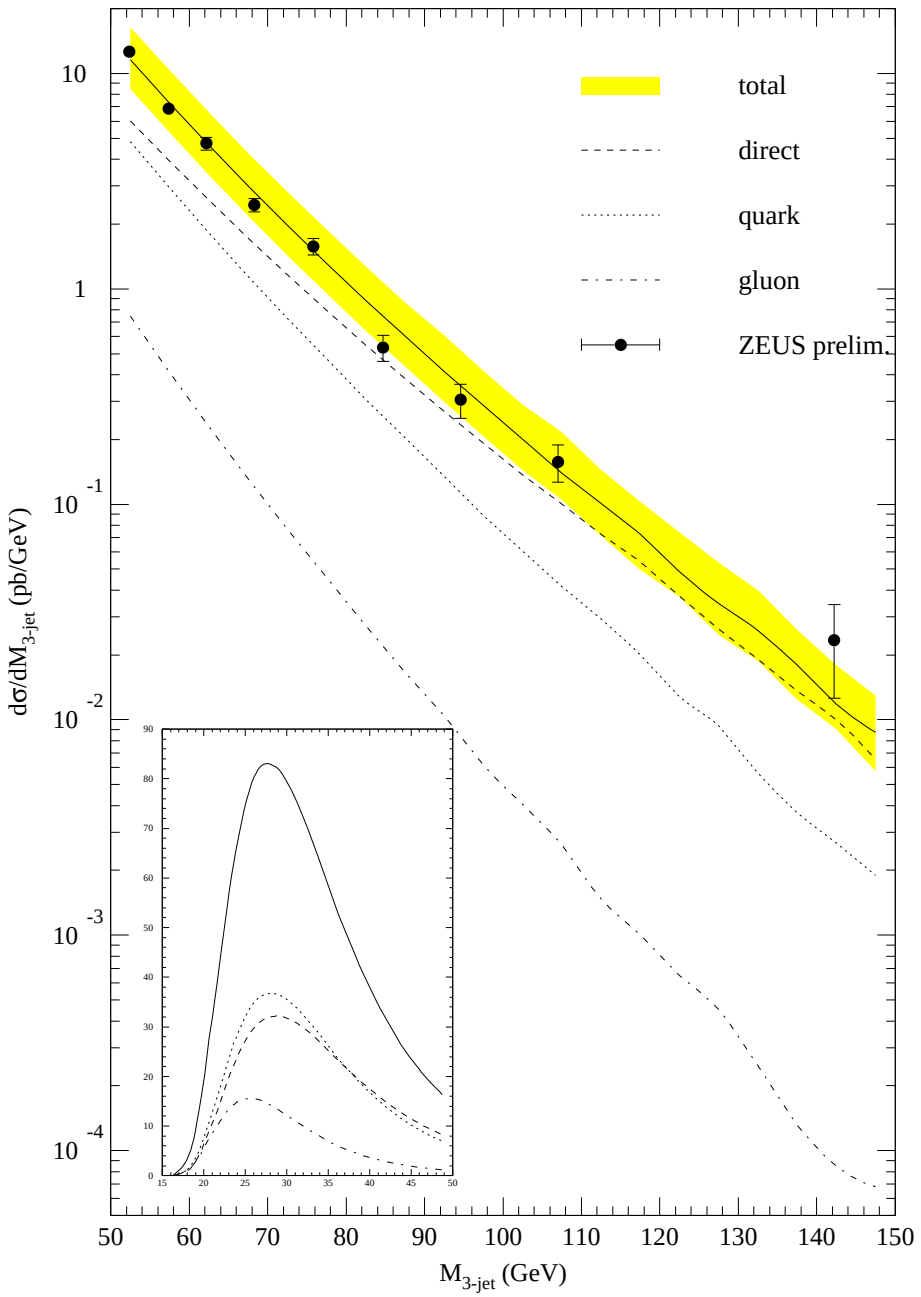

Fig. 3. Total cross section (full curve) for the photoproduction of three jets as a function of the three jet mass $M_{3-\mathrm{jet}}$. We also show the variation of the absolute normalization due to the uncertainty in the scale choice (shaded band) and the contributions from direct photons (dashed), quarks (dotted), and gluons (dot-dashed) in the photon. The ZEUS data [11] agree well with the QCD prediction [12]

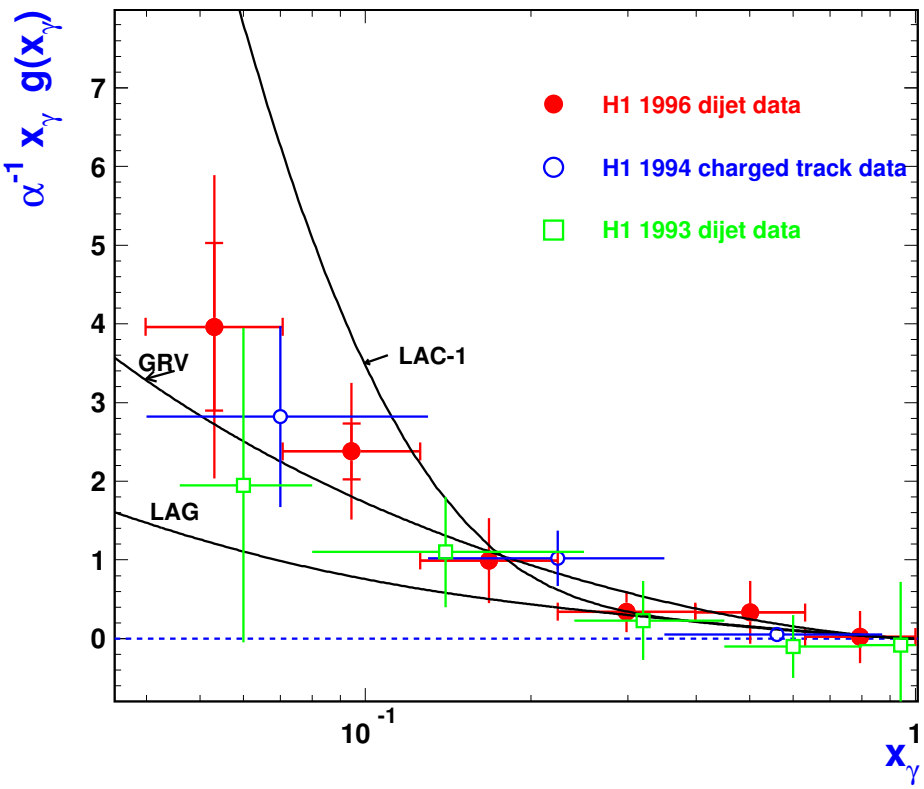

Fig. 4. H1 extraction of the gluon density in the photon from 1996 dijet data [13], 1994 charged track data [14], and 1993 dijet data [15]. The data are consistent with each other and with LO GRV parametrization [16]. The 1996 data rule out both the LAC1 [17] and LAG [18] gluon parametrizations

the hadronization process can be obtained in the production of single hadrons, which is described theoretically by fragmentation functions. Prior to the last Ringberg HERA workshop, several new NLO QCD fits of fragmentations functions for charged pions, charged kaons, and neutral kaons to e^+e^- data from TPC, ALEPH, and Mark II had been performed. They had been applied to a NLO QCD calculation for photoproduction and successfully been compared to HERA data [19]. Since then, fragmentation functions for heavy particles, such as $D^{*\pm}$ and B mesons, have been fitted to ALEPH and OPAL data, and they also compare favorably to HERA data (see contribution by G. Kramer to these proceedings). A new fit of charged pion, charged kaon, and proton fragmentation functions, separately for light flavors, heavy flavors, and gluons, to new LEP and SLC data is currently in progress [20].

In Fig. 5 we compare NLO QCD predictions for the rapidity distribution of charged hadrons [21] to recent H1 data [14]. Good agreement is found for

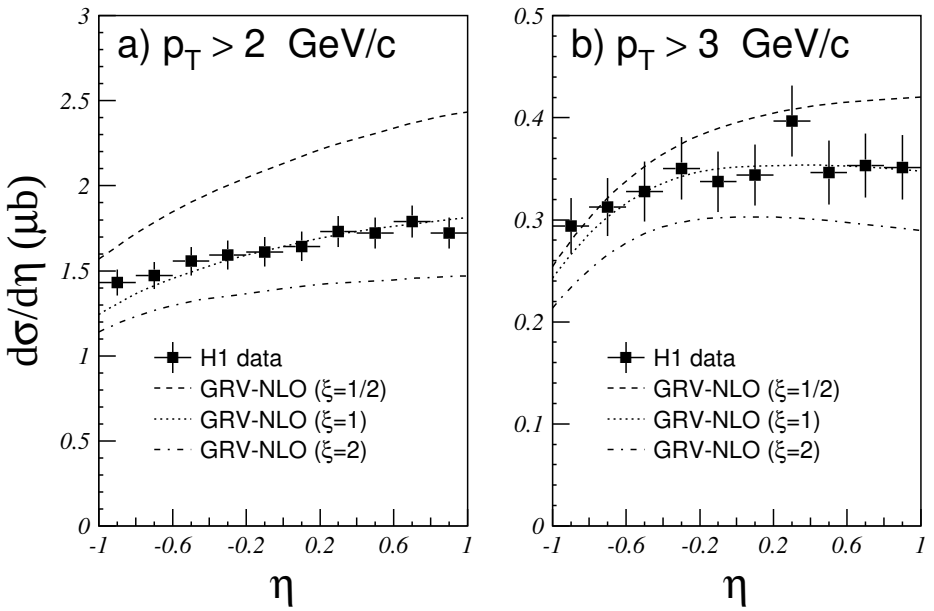

Fig. 5. Differential cross section for the photoproduction of charged hadrons as a function of rapidity for two different transverse momentum cuts. Recent H1 data [14] are compared to NLO QCD predictions [21] with three different scale choices

the GRV parton densities in the photon [16] and the proton [22] and a central scale choice of $\mu = M_\gamma = M_p = p_T$, but the theoretical scale uncertainty in NLO QCD is still considerable. It is worth noting that in inclusive hadron production, perturbative QCD works remarkably well down to very low transverse momenta of $p_T > 2$ or 3 GeV. There is no excess in the forward η region as observed in jet photoproduction. Thus, inclusive hadron production offers the potential to extract the gluon density in the photon in low-p_T (and therefore low-x_γ) cross section measurements.

It is also interesting to check the universality of fragmentation functions and the factorization theorem in photoproduction experiments. In Fig. 6 we show a recent ZEUS fragmentation function measurement for charged hadrons [23], measured in photoproduced jets with $E_T > 8$ GeV, $|\eta| < 0.5$, and $R = 1$, which agrees nicely with the NLO QCD fit to e^+e^- data [21]. The error band in the NLO QCD fit comes from a variation of the fragmenting quark flavor, which is unknown in the ZEUS analysis.

4 Prompt Photons

Prompt photon production was not discussed at the 1997 Ringberg HERA workshop – it had yet to be observed. Only recently have H1 and ZEUS reported

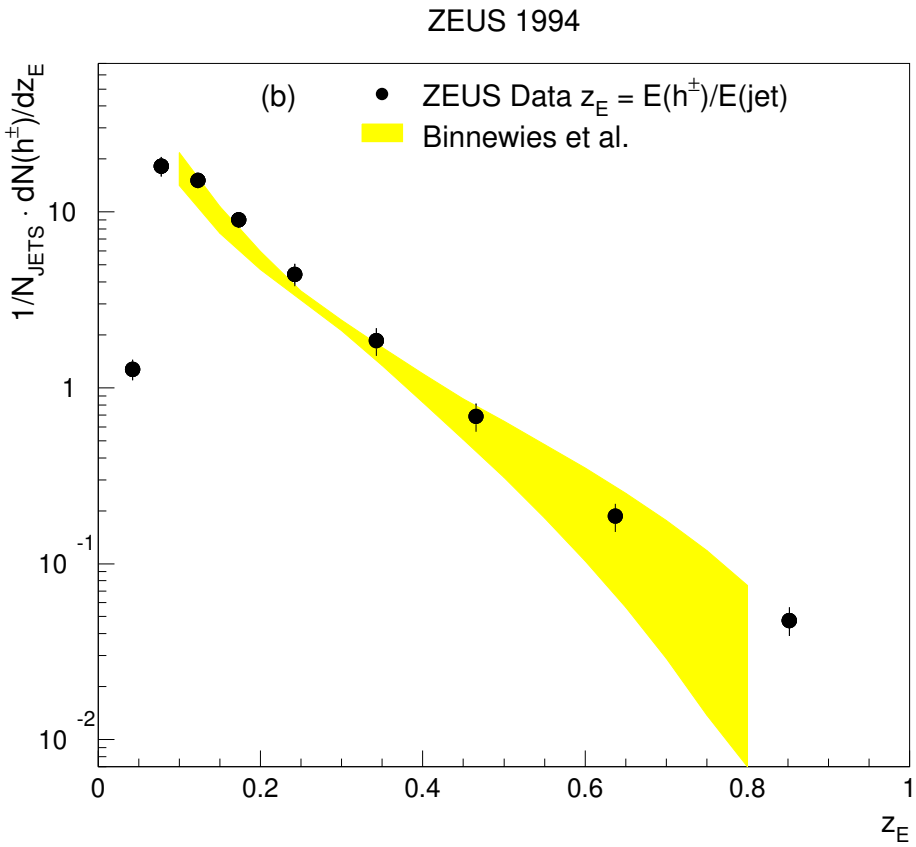

Fig. 6. Fragmentation function of charged particles as a function of their longitudinal momentum fraction. The ZEUS data [23] for particles within photoproduced jets are compared to a NLO fit to e^+e^- data [21]

results on this process [24,25] and have two NLO QCD calculations for isolated photon production and for the production of a photon in association with a jet become available [3,26]. These two calculations differ in their powercounting of the strong coupling constant and in their consideration of higher-order corrections. To illustrate this, we have listed in Fig. 7 the direct, single-resolved, and double-resolved diagrams for photoproduction of prompt photons. The single-resolved process includes either photon structure or photon fragmentation contributions, whereas in the double-resolved case the initial and final state photons contribute both through their partonic constituents. Gordon counts the photon structure and fragmentation functions as $\mathcal{O}(\alpha/\alpha_s)$ from considering the asymptotic limit and calculates the NLO corrections to all three types of subprocesses. Krawczyk *et al.* count the photon structure as $\mathcal{O}(\alpha)$, calculate the NLO corrections only to the direct process, and in addition take into account the box

DIAGRAM	GORDON	KRAWCZYK ET AL.
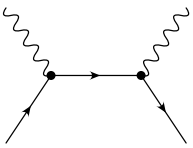	$O(\alpha^2)$ LO+NLO	$O(\alpha^2)$ LO+NLO
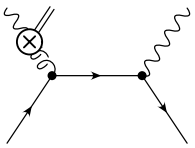	$O(\alpha\alpha_s)O(\alpha/\alpha_s)=O(\alpha^2)$ LO+NLO	$O(\alpha\alpha_s)O(\alpha)=O(\alpha^2\alpha_s)$ (N)LO
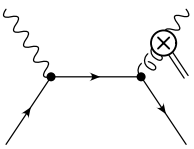	$O(\alpha\alpha_s)O(\alpha/\alpha_s)=O(\alpha^2)$ LO+NLO	$O(\alpha\alpha_s)O(\alpha)=O(\alpha^2\alpha_s)$ (N)LO
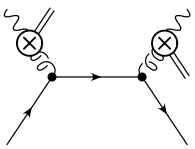	$O(\alpha_s^2)O(\alpha^2/\alpha_s^2)=O(\alpha^2)$ LO+NLO	$O(\alpha_s^2)O(\alpha^2)=O(\alpha^2\alpha_s^2)$ (NN)LO
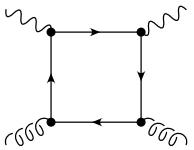	$O(\alpha^2\alpha_s^2)$ --	$O(\alpha^2\alpha_s^2)$ NNLO

Fig. 7. Diagrammatic comparison of two prompt photon QCD calculations. Gordon calculates the NLO corrections to the direct, single-resolved, and double-resolved contributions [3], whereas Krawczyk *et al.* only calculate the corrections to the direct contribution [26]. On the other hand, Krawczyk *et al.* take into account the box diagram that arises at NNLO

diagram in the last line of Fig. 7. Although the box diagram is formally of NNLO, it is known to have a large numerical contribution. This is demonstrated in Fig. 8 where we compare the calculation by Krawczyk *et al.* using GRV photon [16] and proton [22] structure and photon fragmentation functions [27] to ZEUS data for the production of isolated photons with $E_T > 5$ GeV [28]. With higher luminosity and the ensuing better accuracy of the data, prompt photon production at HERA will eventually provide useful tests of photon structure and fragmentation functions.

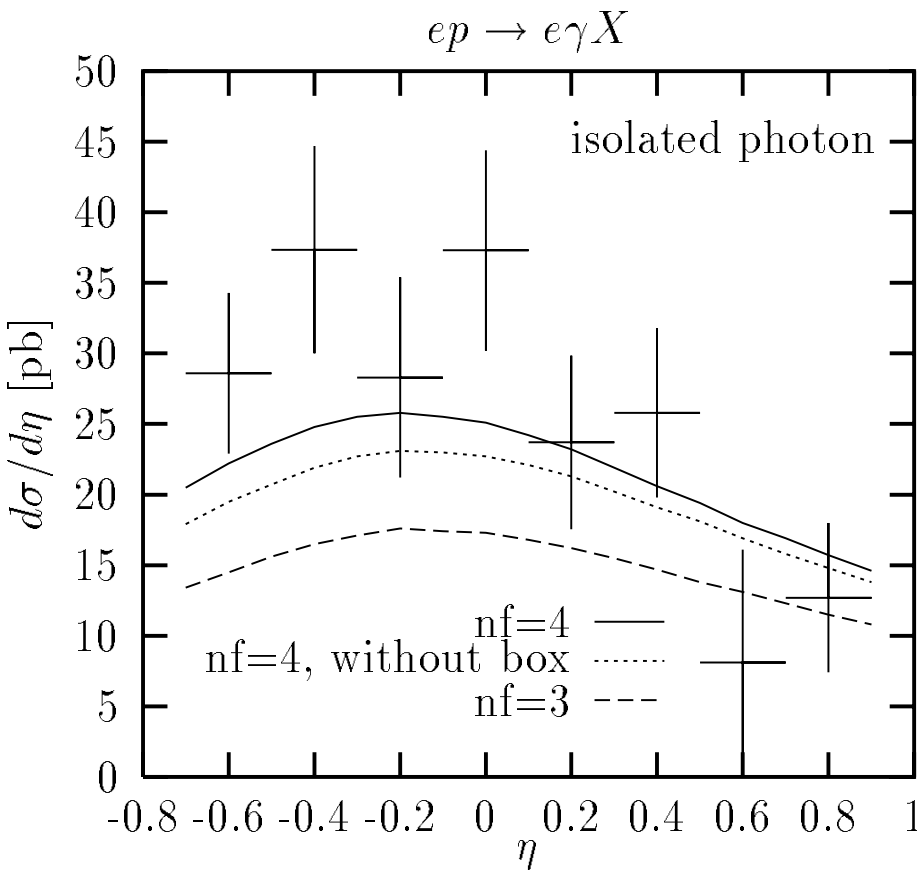

Fig. 8. Differential cross section for the photoproduction of a photon of transverse energy $E_T \in [5;10]$ GeV, which is isolated in a cone with radius $R = 1$ and hadronic transverse energy fraction $\epsilon = 0.1$, as a function of rapidity. The ZEUS data [28] are compared to QCD predictions with and without the NNLO box diagram and with three and four quark flavors [26]

5 Summary

In summary, hard photoproduction processes can provide very useful information on the hadronic structure of the photon, in particular on the gluon density, which is complimentary to the information coming from deep inelastic photon-photon scattering at electron-positron colliders. Among the different hadronic final states, jets are most easily accessible experimentally and phenomenologically. On the other hand, inclusive hadron production offers the possibility to test the universality of hadron fragmentation functions and measure the photon structure down to very low values of p_T and x_γ. Prompt photon production suf-

fers from a reduced cross section and limited data, but allows for the additional testing of photon fragmentation functions.

Acknowledgment. I would like to thank the organizers of the Ringberg workshop for the kind invitation. This work has been supported by the U.S. Department of Energy under Contract W-31-109-ENG-38.

References

1. M. Klasen, T. Kleinwort and G. Kramer, Eur. Phys. J. Direct **C1** (1998) 1 and references therein
2. B.A. Kniehl and G. Kramer, Z. Phys. **C62** (1994) 53 and references therein
3. L.E. Gordon, Phys. Rev. **D57** (1998) 235 and references therein
4. M. Klasen, hep-ph/9706292 and references therein
5. J.M. Butterworth, L. Feld, M. Klasen and G. Kramer, hep-ph/9608481
6. M. Klasen and G. Kramer, Phys. Rev. **D56** (1997) 2702
7. J.E. Huth *et al.*, *Presented at Summer Study on High Energy Physics, Research Directions for the Decade, Snowmass, CO, Jun 25 - Jul 13, 1990*
8. S.D. Ellis and D.E. Soper, Phys. Rev. **D48** (1993) 3160
9. J. Breitweg *et al.* [ZEUS Collaboration], hep-ex/9905046
10. B.W. Harris, M. Klasen and J. Vossebeld, hep-ph/9905348
11. J. Breitweg *et al.* [ZEUS Collaboration], Phys. Lett. **B443** (1998) 394
12. M. Klasen, Eur. Phys. J. **C7** (1999) 225
13. J. Cvach [H1 Collaboration], hep-ex/9906012
14. C. Adloff *et al.* [H1 Collaboration], hep-ex/9810020
15. T. Ahmed *et al.* [H1 Collaboration], Nucl. Phys. **B445** (1995) 195
16. M. Glück, E. Reya and A. Vogt, Phys. Rev. **D46** (1992) 1973
17. H. Abramowicz, K. Charchula and A. Levy, Phys. Lett. **B269** (1991) 458
18. H. Abramowicz, E. Gurvich and A. Levy, Phys. Lett. **B420** (1998) 104
19. B.A. Kniehl, hep-ph/9709261 and references therein
20. B.A. Kniehl, G. Kramer, and B. Pötter, to be published
21. J. Binnewies, B.A. Kniehl and G. Kramer, Phys. Rev. **D52** (1995) 4947
22. M. Glück, E. Reya and A. Vogt, Z. Phys. **C53** (1992) 127
23. J. Breitweg *et al.* [ZEUS Collaboration], Eur. Phys. J. **C2** (1998) 77
24. J. Breitweg *et al.* [ZEUS Collaboration], Phys. Lett. **B413** (1997) 201
25. K. Muller, *In *Jerusalem 1997, High energy physics* 464-467*
26. M. Krawczyk and A. Zembrzuski, hep-ph/9810253
27. M. Glück, E. Reya and A. Vogt, Phys. Rev. **D48** (1993) 116
28. L.E. Sinclair [ZEUS Collaboration], hep-ex/9810044